APL Photonics

Diffraction-induced enhancement of optical spin Hall effect in a dielectric grating

Cite as: APL Photonics 5, 066106 (2020); https://doi.org/10.1063/5.0009616
Submitted: 01 April 2020 • Accepted: 29 May 2020 • Published Online: 18 June 2020

Minkyung Kim, Dasol Lee, Byoungsu Ko, et al.

Diffraction-induced enhancement of optical spin Hall effect in a dielectric grating

Cite as: APL Photon. 5, 066106 (2020); doi: 10.1063/5.0009616
Submitted: 1 April 2020 • Accepted: 29 May 2020 •
Published Online: 18 June 2020

Minkyung Kim,[1] Dasol Lee,[1] Byoungsu Ko,[1] and Junsuk Rho[1,2,a)]

AFFILIATIONS

[1]Department of Mechanical Engineering, Pohang University of Science and Technology (POSTECH), Pohang 37673, South Korea
[2]Department of Chemical Engineering, Pohang University of Science and Technology (POSTECH), Pohang 37673, South Korea

[a)]**Author to whom correspondence should be addressed:** jsrho@postech.ac.kr

ABSTRACT

The enhancement of the optical spin Hall effect (OSHE) of a transmitted beam has been achieved in a small incident angle of a sub-degree scale. The OSHE at a large incident angle can be beneficial in optical applications, such as polarization-dependent sensors and filters, but studies to increase the OSHE at a large incident angle have been elusive in transmission mode. We propose a dielectric grating on a metal layer to achieve the grating-induced increase of the OSHE. The polarization-dependent transmission and OSHE that reaches several wavelengths are numerically demonstrated. We also show the tunability of the operating wavelength and incident angle of the OSHE by changing materials and geometrical parameters.

I. INTRODUCTION

Electrons that possess opposite spin may undergo transverse shift along the opposite direction even in the absence of an external magnetic field.[1,2] This spin-dependent deflection of electrons known as the spin Hall effect is not a unique phenomenon that can only be found in electronic systems, but has analogies in photonics in terms of spin-dependent phenomena, such as transverse splitting,[3,4] angular splitting,[5,6] and splitting of exciton–polaritons.[7,8] Among them, the optical spin Hall effect (OSHE), also known as the photonic spin Hall effect and spin Hall effect of light, manifests itself as a spin-dependent and transverse splitting of circularly polarized light at an interface between two media,[3,4,9] and is also known as the Imbert–Fedorov effect.[10,11] The physical origin of the OSHE lies on the finite beam waist of the incident beam, which contains not only central wave vector components, but also other wave vectors slightly deflected from the central beam axis in both in-plane and out-of-plane directions with respect to the incident plane. The deflected wave vectors have different incident angles and incident planes. Therefore, the wave vector deflection results in the deviation of polarization basis, and thereby induces a positive geometric phase for one circular polarization and a negative geometric phase for the other.

OSHE is a universal phenomenon that occurs at an interface between natural media[4,10–13] and random media.[14] In general, the amount of shift is small corresponding to a fraction of the wavelength. OSHE can be increased by exploiting structured media that transmit or reflect *s*- and *p*-polarization differently, such as metamaterials,[15–19] metasurfaces,[20–22] and two-dimensional (2D) materials.[23–27] Alternatively, OSHE can be significantly increased under a specific circumstance in which the transmission or reflection of only one polarization vanishes. One example is reflection near the Brewster angle.[12,13] In contrast, previous studies to increase OSHE in the transmission type have mainly focused on a small incident angle, on the order of milli-radians, in which OSHE is significantly enhanced as the incident angle goes to zero.[17,18,28,29] The enhancement of OSHE at a large incident angle has not been proposed in a transmission type.

Here, we present OSHE in a dielectric grating on a metal film by maximizing the difference between the transmission coefficients of *s*-polarization and those of *p*-polarization. The metal film impedes light transmission except the *p*-polarized first-order diffracted mode that is coupled to surface plasmon polaritons (SPPs). We numerically demonstrate that these polarization-dependent transmission coefficients lead to high OSHE at a large incident angle, whereas the OSHE is enhanced at a small incident angle in previous

instances. We further show that the operating wavelength or incident angle of the OSHE can be tuned by changing materials or geometrical parameters of a device. The diffraction-induced OSHE will be advantageous in optical applications, including filters and sensors.

II. RESULTS AND DISCUSSION

A. Principle and design

A vertically polarized incident beam that transmits at an optical interface is shifted by an amount of δ given as[28] [Fig. 1(a)]

$$\delta^{\pm} = \pm \frac{\cot\theta_i}{k_1} \mathrm{Re}\left(1 - \frac{t_p}{t_s}\right) \tag{1}$$

assuming that the beam waist ω_0 is sufficiently large [$(k_1\omega_0/\cot\theta_i)^2 \gg 1$]. Here, k_1 is a wave vector in medium 1, θ_i is an incident angle, t_s and t_p are transmission coefficients for s- and p-polarization, respectively, + denotes left circular polarization and − denotes right circular polarization.

Equation (1) implies that OSHE can be increased in two ways, either by reducing θ_i or by increasing the difference between t_s and t_p. However, reducing θ_i does not always make δ increase. At an interface between natural materials, δ decreases as θ_i decreases[4] because t_s/t_p (or t_p/t_s) converges more rapidly to unity than $\cot\theta_i$ diverges. In contrast, OSHE generally increases at small θ_i ($\ll\pi/2$) in artificially structured media[17,18,28,29] as a result of the diverging behavior of $\cot\theta_i$. This term is associated with the short length of the adiabatic path in the momentum space [Fig. 1(b)]. OSHE can be understood to be a consequence of the geometric phase Φ_B that is acquired by a deflected wave vector in the polarization space.[9,30,31] The deflected wave vector dk that is perpendicular to the incident plane alters both the incident plane and the polarization basis [Fig. 1(b)]. For a given dk, the angular deflection $\Phi = dk/(k\sin\theta_i)$ in the momentum space increases as θ_i decreases [insets in Figs. 1(b) and 1(c)]. Increase in Φ directly yields the increased geometric phase as[32] $\Phi_B = \Phi\cos\theta_i \propto \cot\theta_i$. Thus, δ, which is closely related to the gradient of the geometric phase,[33,34] has the $\cot\theta_i$ term, which diverges as θ_i converges to zero. Therefore, the remarkable enhancement of OSHE has been demonstrated in a narrow range of θ_i within a fraction of a degree of 0°,[17,18,28,29] in which δ changes drastically in response to θ_i. Despite the significant increase of δ, the high sensitivity complicates the task of fine controlling the shift. Moreover, sometimes a large OSHE at large θ_i is preferable [Fig. 1(c)], for example, for applications such as polarization-dependent filters and beam splitters. Thus, a new route to attain large OSHE without relying on the short path length in the momentum space is in demand.

To increase OSHE without reducing θ_i, we focus on the other term t_p/t_s. We propose a dielectric grating on a metal film [Fig. 2(a)] to achieve polarization-dependent diffraction. The grating and substrate are silicon dioxide (SiO_2) and the metal is gold (Au). The geometric parameters of the grating are as follows: period p = 700 nm, width $w = p/2$, and height H = 100 nm. The thickness of the metal layer is t_m = 60 nm, which is much thicker than the skin depth of metal in the visible spectrum. We first examine the SPPs of the SiO_2–Au–air interface. Their dispersion curve can be obtained by solving two boundary conditions of p-polarized modes at the three-layer structure as[35]

$$e^{-2k_m t_m} = \frac{k_m/\varepsilon_m + k_d/\varepsilon_d}{k_m/\varepsilon_m - k_d/\varepsilon_d} \times \frac{k_m/\varepsilon_m + k_a/\varepsilon_a}{k_m/\varepsilon_m - k_a/\varepsilon_a}. \tag{2}$$

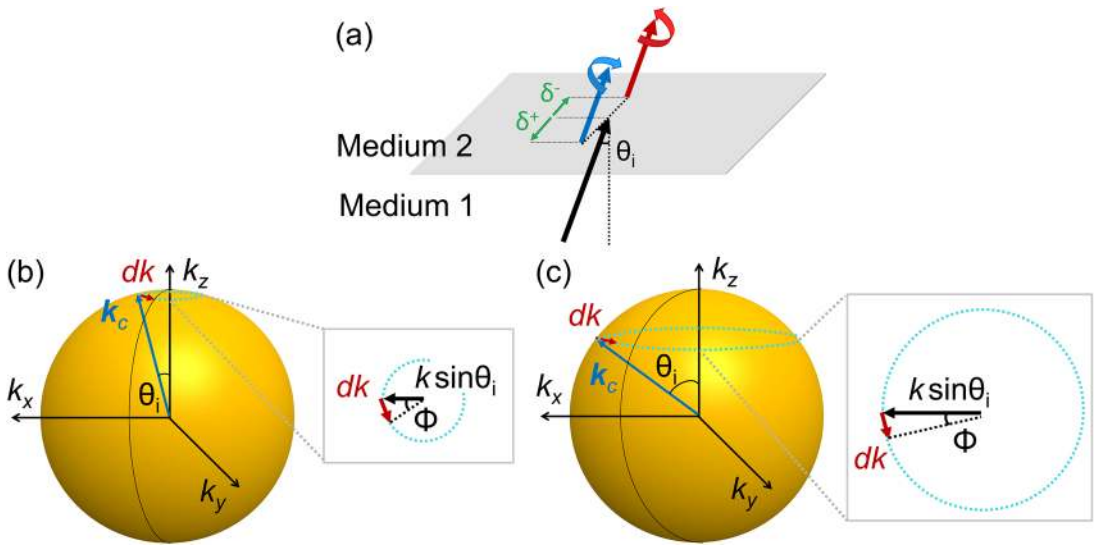

FIG. 1. Schematics of the optical spin Hall effect in a (a) real space and [(b) and (c)] momentum space. The gray panel represents an optical interface between Medium 1 and Medium 2. The black arrow indicates the linearly polarized incident Gaussian beam. Red and blue arrows denote the circularly polarized transmitted beam with opposite handednesses. [(b) and (c)] Optical spin Hall effect in a momentum space when θ_i is (b) small and (c) large. dk denotes the wave vector component deflected perpendicular to the incident plane. Insets show a loop of the adiabatic path associated with the wave vector deflection. The radius of the loop is $k\sin\theta_i$. The geometric phase Φ_B of the deflected beam is directly proportional to Φ, which is an azimuthal angle of dk. Thus, a small θ_i gives rise to a large Φ_B for a fixed dk.

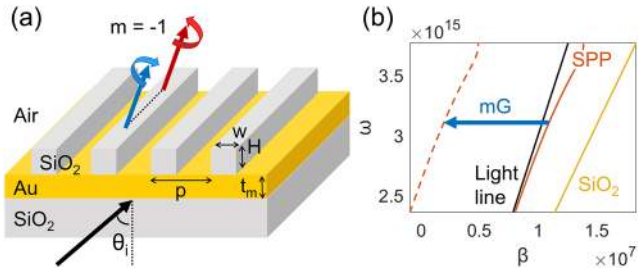

FIG. 2. Illustration of a sample and dispersion curve of SPPs. (a) A schematic of a grating. Dielectric grating is periodically arranged on a metal film deposited on a substrate. Geometric parameters are given as p = 700 nm, $w = p/2$, H = 100 nm, and t_m = 60 nm. We use SiO_2 as the dielectric and Au as the metal. The black arrow indicates the incident Gaussian beam and while red and blue arrows denote circularly polarized transmitted beams. (b) Dispersion curve of SPPs at the SiO_2–Au–air interface (red solid) and the bulk dispersion of air (black) and SiO_2 (yellow). SPPs have a wave vector higher than that of light and cannot be transmitted to air. This phase mismatch can be compensated for by using mG where $m = -1$.

Here, ε denotes relative permittivity, $k_n = \sqrt{\beta^2 - k_0^2\varepsilon_n}$, where the subscripts denote $n = m$ for metal, $n = d$ for dielectric, $n = a$ for air; β is the propagation constant and k_0 is the wave vector in the free space. The dispersion relationship of SPPs can be obtained by solving Eq. (2) in terms of β.

The dispersion curve of SPPs has a higher wave vector component than light [Fig. 2(b)]. Thus, light that is incident obliquely from the substrate can excite the SPPs, but they cannot be coupled to air and remain evanescent. Grating can compensate for this phase mismatch and allow the transmission of the p-polarized incidence. The phase matching condition of grating is applied to p-polarization as[35]

$$k_1 \sin\theta_i + mG = k_2 \sin\theta_t, \tag{3}$$

where m is the diffraction order, $G = 2\pi/p$ is the reciprocal vector of the grating, θ_t is a transmitted angle, and k_2 is a wave vector in the outer medium, which is air in this case. Whereas SPPs have a wave vector that is higher than that of light, $m = -1$ mode [red dashed curve, Fig. 2(b)] falls inside the light line and can be coupled to air. Because the phase compensation using a grating only occurs for p-polarization and the SPPs exist only for p-polarization, the transmission of $m = -1$ mode appears for p-polarization, whereas most of the s-polarized incidence cannot be transmitted by any mode because of the thick metal layer and lack of the coupling mechanism. This polarization-dependent transmission contributes strongly to the increase in OSHE at large θ_i.

B. Numerical demonstration of OSHE

To numerically demonstrate polarization-dependent transmission, the transmission coefficients of diffraction order $m = -1$ for p- and s-polarization were calculated using COMSOL Multiphysics (Fig. 3). The kinks highlighted as blue curves are not numerical artifacts, but Rayleigh anomalies that universally appear in grating structures at the transition between propagating and evanescent modes.[36] To simulate transmission under oblique incidence, 2D

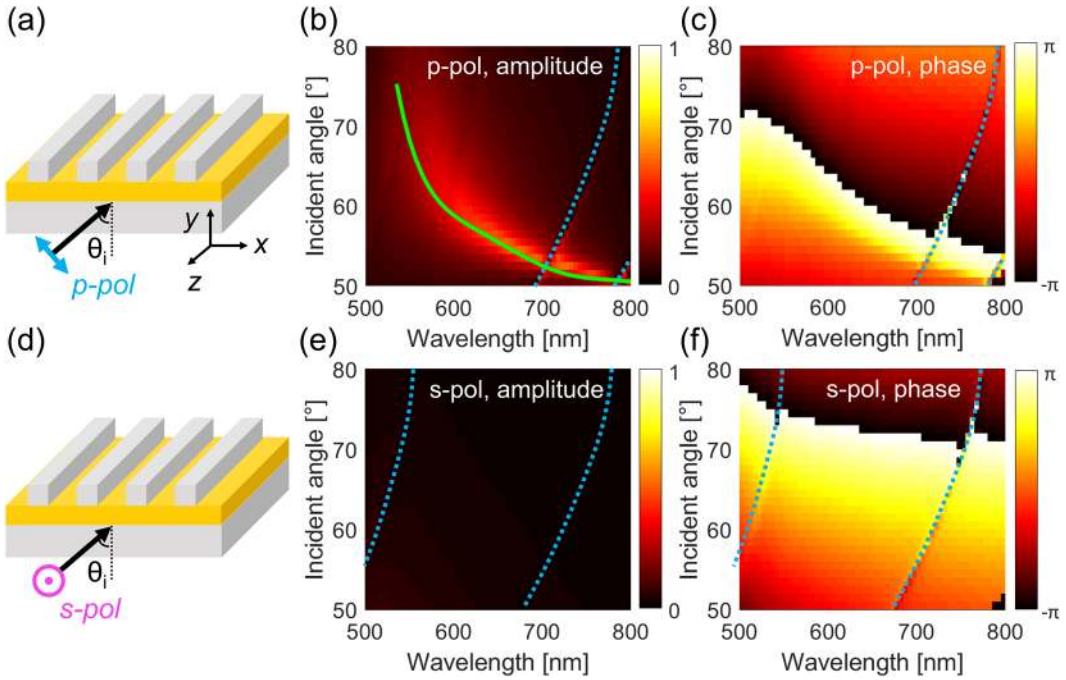

FIG. 3. Transmission coefficients for [(a)–(c)] p- and [(d)–(f)] s-polarization when the diffraction order is $m = -1$. The green solid curve highlights the peak of $|t_s| < 0.1$. The blue dashed curves indicate Rayleigh anomalies.

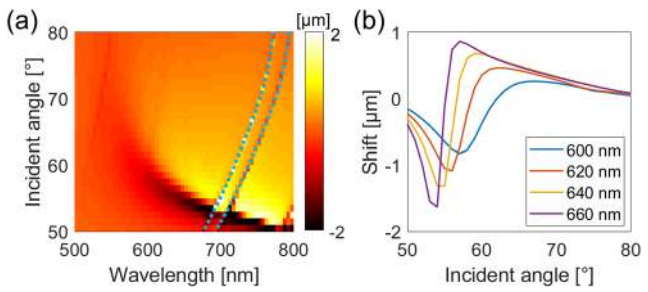

FIG. 4. Shift for vertical polarization. (a) Incident angle and wavelength dependent shift in the micrometer scale. (b) Incident angle dependence of the shift at specific wavelengths.

simulation was performed in the x–y plane, in which the boundaries that are normal to the x-axis are set as the Bloch boundary condition. To obtain $m = -1$ mode, we focus on a large incident angle in the range of $50^\circ \le \theta_i \le 80^\circ$. In this range, Eq. (3) has no real solution of θ_t for $m = 0$, while has a real solution for $m = -1$. The polarization-dependent phase compensation leads to a transmission peak of diffracted light ($m = -1$) only for p-polarization [Figs. 3(a) and 3(b)]. For a given θ_i, the p-polarized incidence is converted to SPPs at a wavelength that satisfies the phase matching [Eq. (3)]. The SPPs, which are localized at the interfaces, become radiative because of the phase compensation of the grating. The peak has a maximum value of 0.52 and appears in a broad range of visible wavelengths [green solid curve, Fig. 3(b)]. In contrast, under s-polarized incidence [Fig. 3(d)], SPPs are not excited and phase compensation by the grating does not occur. Thus, transmission is small ($|t_s| < 0.1$) and has no prominent feature [Figs. 3(d) and 3(e)]. This polarization-dependent transmission increases the term $1 - t_p/t_s$ in Eq. (1), thereby resulting in the enhancement of OSHE. The phases of transmission coefficients [Figs. 3(c) and 3(f)] are plotted because their phase difference also influences δ according to Eq. (1).

We calculate δ by using the simulated transmission coefficients and Eq. (1) [Fig. 4(a)]. As expected from Eq. (1), δ exhibits a similar peak with t_p at a broad range of $50^\circ \le \theta_i \le 80^\circ$. The maximum shift in a given parameter space is approximately 3.7 μm at $\lambda = 730$ nm and $\theta_i = 63^\circ$, which corresponds to 5.1λ for $\delta > 0$, and -3.5 μm at $\lambda = 800$ nm and $\theta_i = 50^\circ$, which corresponds to 4.4λ for $\delta < 0$. To see more clearly, δ at specific wavelengths are shown in Fig. 4(b). Wavelengths are selected in the range of 600 nm $\le \lambda \le$ 660 nm to avoid the kinks that originate from Rayleigh anomalies [blue curves, Fig. 4(a)]. δ exhibits the resonant feature near the wavelength satisfying the phase matching condition. The operating incident angle can be tuned by changing the wavelength of interest. The results of the three-dimensional full-wave simulation at $\lambda = 640$ nm and $\lambda = 660$ nm can be found in the supplementary material.

The efficiency of the optical spin Hall effect is low as a result of the low transmission of s-polarized incidence. The amplitude of electric field of the transmitted beam divided by that of the incidence is equal to $|t_s|$, which has a maximum value of 0.074 in the given parameter space. The efficiency can be increased by reducing t_m. The transmission of the proposed system and a system with a thinner metal layer can be found in the supplementary material.

C. Tunability of operating wavelength and incident angle range

The operating wavelength and incident angle of OSHE are closely related to the structural peak of $|t_p|$. The shape of the peak is determined by the phase matching condition of SPP dispersion, in which the refractive indices of metal and dielectric and geometrical parameters are important. Therefore, changing the materials or the geometrical parameters may alter the operating wavelength and incident angle. Because δ shares the same structural peak with $|t_p|$, we plot the peak of $|t_p|$ in three additional systems to demonstrate the tunability of OSHE (blue curves, Fig. 5).

For the first additional system, we replaced Au with silver (Ag) while keeping the other materials and geometrical parameters the same [Fig. 5(a)]. The wavelength range of the enhanced OSHE widened, ranging from 400 nm to 800 nm. The peak θ_i of a given wavelength also differed as a result of the change in SPPs dispersion. At a fixed wavelength in the visible regime, the real part of permittivity is lower for Ag than that for Au. Thus, considering that SiO_2 has constant-like permittivity, the excitation of SPPs and their conversion to radiative waves occurs at a lower wavelength for a given θ_i. Second, we changed the dielectric from SiO_2 to aluminum oxide (Al_2O_3) for both the grating and the substrate [Fig. 5(b)].

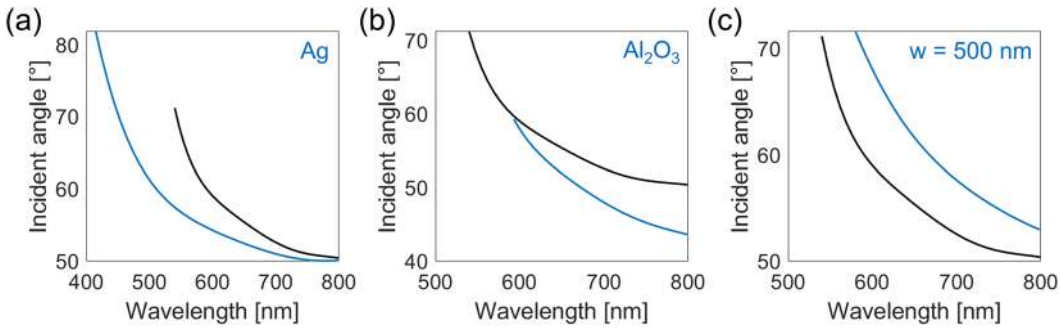

FIG. 5. Tunability of OSHE in three different systems. The peak of $|t_p|$ when (a) Au is replaced by Ag, (b) SiO_2 is replaced by Al_2O_3, and (c) w = 500 nm. Black curves correspond to the $|t_p|$ peak of the original system as a reference.

The dispersion of SPPs at the Al_2O_3–Au–air interface is similar to that at the SiO_2–Au–air interface according to Eq. (2). Instead, the higher refractive index of Al_2O_3 than that of SiO_2 results in a peak at the smaller θ_i for a fixed wavelength. Last, we changed the grating width from $w = 350$ nm to $w = 500$ nm while keeping the other parameters fixed [Fig. 5(c)]. Although the role of the duty cycle cannot be explained by the phase matching [Eq. (3)], larger w increases the contact area of the Au film with the dielectric grating and alters SPPs dispersion to have larger β for a given wavelength. The increase in w led to a red shift of $|t_p|$.

III. CONCLUSION

In conclusion, we numerically demonstrate that diffraction induces the enhancement of OSHE at a large incident angle by exploiting a dielectric grating on a metal film. The polarization-dependent behavior of the grating and surface plasmon polaritons that only occur for p-polarization results in amplified shift that reaches several wavelengths. We demonstrate that the enhancement of the optical spin Hall effect does not necessarily require a short path length in the momentum space. The large OSHE at a large incident angle will facilitate polarization-sensitive optical devices, such as switches and beam splitters.

SUPPLEMENTARY MATERIAL

See the supplementary material for the three-dimensional direct simulation results and analysis on the efficiency.

AUTHORS' CONTRIBUTIONS

J.R., M.K., and D.L. conceived the idea and initiated the project. M.K. conducted numerical simulations. M.K. and D.L. mainly wrote the manuscript. M.K., D.L., and B.K. analyzed the data. All authors participated in the discussion and confirmed the final manuscript. J.R. guided the entire project. M.K. and D.L. contributed equally to this work.

ACKNOWLEDGMENTS

This work was financially supported by the National Research Foundation (NRF) (Grant Nos. NRF-2019R1A2C3003129, CAMM-2019M3A6B3030637, and NRF-2019R1A5A8080290) funded by the Ministry of Science and ICT (MSIT) of the Korean government. M.K. acknowledges the Global Ph.D. fellowship (Grant No. NRF-2017H1A2A1043204) from NRF-MSIT of the Korean government.

DATA AVAILABILITY

The data that support the findings of this study are available from the corresponding author upon reasonable request.

REFERENCES

[1]M. I. Dyakonov and V. Perel, "Possibility of orienting electron spins with current," J. Exp. Theor. Phys. **13**, 467 (1971).
[2]M. I. Dyakonov and V. Perel, "Current-induced spin orientation of electrons in semiconductors," Phys. Lett. A **35**, 459–460 (1971).
[3]M. Onoda, S. Murakami, and N. Nagaosa, "Hall effect of light," Phys. Rev. Lett. **93**, 083901 (2004).
[4]O. Hosten and P. Kwiat, "Observation of the spin Hall effect of light via weak measurements," Science **319**, 787–790 (2008).
[5]N. Shitrit, I. Bretner, Y. Gorodetski, V. Kleiner, and E. Hasman, "Optical spin Hall effects in plasmonic chains," Nano Lett. **11**, 2038–2042 (2011).
[6]L. Huang, X. Chen, B. Bai, Q. Tan, G. Jin, T. Zentgraf, and S. Zhang, "Helicity dependent directional surface plasmon polariton excitation using a metasurface with interfacial phase discontinuity," Light: Sci. Appl. **2**, e70 (2013).
[7]A. Kavokin, G. Malpuech, and M. Glazov, "Optical spin Hall effect," Phys. Rev. Lett. **95**, 136601 (2005).
[8]C. Leyder, M. Romanelli, J. P. Karr, E. Giacobino, T. C. Liew, M. M. Glazov, A. V. Kavokin, G. Malpuech, and A. Bramati, "Observation of the optical spin Hall effect," Nat. Phys. **3**, 628–631 (2007).
[9]X. Ling, X. Zhou, K. Huang, Y. Liu, C.-W. Qiu, H. Luo, and S. Wen, "Recent advances in the spin Hall effect of light," Rep. Prog. Phys. **80**, 066401 (2017).
[10]F. I. Fedorov, "To the theory of total reflection," Dokl. Akad. Nauk SSSR **105**, 465–468 (1955).
[11]C. Imbert, "Calculation and experimental proof of the transverse shift induced by total internal reflection of a circularly polarized light beam," Phys. Rev. D **5**, 787 (1972).
[12]J. B. Götte, W. Löffler, and M. R. Dennis, "Eigenpolarizations for giant transverse optical beam shifts," Phys. Rev. Lett. **112**, 233901 (2014).
[13]X. Qiu, Z. Zhang, L. Xie, J. Qiu, F. Gao, and J. Du, "Incident-polarization-sensitive and large in-plane-photonic-spin-splitting at the Brewster angle," Opt. Lett. **40**, 1018–1021 (2015).
[14]T. Bardon-brun, D. Delande, and N. Cherroret, "Spin Hall effect of light in a random medium," Phys. Rev. Lett. **123**, 043901 (2019).
[15]T. Tang, Y. Zhang, J. Li, and L. Luo, "Spin Hall effect enhancement of transmitted light through an anisotropic metamaterial slab," IEEE Photonics J. **9**, 1–10 (2017).
[16]T. Tang, C. Li, and L. Luo, "Enhanced spin Hall effect of tunneling light in hyperbolic metamaterial waveguide," Sci. Rep. **6**, 30762 (2016).
[17]O. Takayama, J. Sukham, R. Malureanu, A. V. Lavrinenko, and G. Puentes, "Photonic spin Hall effect in hyperbolic metamaterials at visible wavelengths," Opt. Lett. **43**, 4602–4605 (2018).
[18]M. Kim, D. Lee, T. H. Kim, Y. Yang, H. J. Park, and J. Rho, "Observation of enhanced optical spin Hall effect in a vertical hyperbolic metamaterial," ACS Photonics **6**, 2530–2536 (2019).
[19]P. V. Kapitanova, P. Ginzburg, F. J. Rodríguez-Fortuño, D. S. Filonov, P. M. Voroshilov, P. A. Belov, A. N. Poddubny, Y. S. Kivshar, G. A. Wurtz, and A. V. Zayats, "Photonic spin Hall effect in hyperbolic metamaterials for polarization-controlled routing of subwavelength modes," Nat. Commun. **5**, 1–8 (2014).
[20]W. Zhu and W. She, "Enhanced spin Hall effect of transmitted light through a thin epsilon-near-zero slab," Opt. Lett. **40**, 2961–2964 (2015).
[21]X. Yin, Z. Ye, J. Rho, Y. Wang, and X. Zhang, "Photonic spin Hall effect at metasurfaces," Science **339**, 1405–1407 (2013).
[22]Y. Liu, X. Ling, X. Yi, X. Zhou, S. Chen, Y. Ke, H. Luo, and S. Wen, "Photonic spin Hall effect in dielectric metasurfaces with rotational symmetry breaking," Opt. Lett. **40**, 756–759 (2015).
[23]W. Zhang, W. Wu, S. Chen, J. Zhang, X. Ling, W. Shu, H. Luo, and S. Wen, "Photonic spin Hall effect on the surface of anisotropic two-dimensional atomic crystals," Photonics Res. **6**, 511–516 (2018).
[24]W. J. M. Kort-Kamp, F. J. Culchac, R. B. Capaz, and F. A. Pinheiro, "Photonic spin Hall effect in bilayer graphene Moiré superlattices," Phys. Rev. B **98**, 195431 (2018).
[25]Z. Cao, X. Liang, X. Qiu, J. Hou, and C. Yang, "Photonic spin Hall effect of graphene hyperbolic metasurfaces in the terahertz region," J. Phys. D: Appl. Phys. **52**, 435104 (2019).
[26]J. Li, T. Tang, L. Luo, and J. Yao, "Enhancement and modulation of photonic spin Hall effect by defect modes in photonic crystals with graphene," Carbon **134**, 293–300 (2018).

[27]H. Lin, B. Chen, S. Yang, W. Zhu, J. Yu, H. Guan, H. Lu, Y. Luo, and Z. Chen, "Photonic spin Hall effect of monolayer black phosphorus in the terahertz region," Nanophotonics **7**, 1929–1937 (2018).
[28]X. Zhou, X. Ling, Z. Zhang, H. Luo, and S. Wen, "Observation of spin Hall effect in photon tunneling via weak measurements," Sci. Rep. **4**, 7388 (2014).
[29]H. Dai, L. Yuan, C. Yin, Z. Cao, and X. Chen, "Direct visualizing the spin Hall effect of light via ultrahigh-order modes," Phys. Rev. Lett. **124**, 053902 (2020).
[30]M. V. Berry, "Quantal phase factors accompanying adiabatic changes," Proc. R. Soc. London, Ser. A **392**, 45–57 (1984).
[31]S. Pancharatnam, "Generalized theory of interference and its applications," Proc. Natl. Acad. Sci., India, Sect. A **44**, 398–417 (1956).
[32]F. Wilczek and A. Shapere, *Geometric Phases in Physics* (World Scientific, 1989), Vol. 5.
[33]K. Y. Bliokh, F. J. Rodríguez-Fortuño, F. Nori, and A. V. Zayats, "Spin–orbit interactions of light," Nat. Photonics **9**, 796 (2015).
[34]X. Ling, X. Zhou, X. Yi, W. Shu, Y. Liu, S. Chen, H. Luo, S. Wen, and D. Fan, "Giant photonic spin Hall effect in momentum space in a structured metamaterial with spatially varying birefringence," Light: Sci. Appl. **4**, e290 (2015).
[35]S. A. Maier, *Plasmonics: Fundamentals and Applications* (Springer Science & Business Media, 2007).
[36]Lord Rayleigh, "On the dynamical theory of gratings," Proc. R. Soc. A **79**, 399–416 (1907).